Characterisation of Nasal Devices for Delivery of Insulin to the Brain and Evaluation in Humans using Functional Magnetic Resonance Imaging

Jed Wingrove[1], Magda Swedrowska[2], Regina Scherließ[3], Mark Parry[4], Mervin Ramjeeawon[4], David Taylor[2], Gregoire Gauthier[5], Louise Brown[6] Stephanie Amiel[7,8] Fernando Zelaya[1], Ben Forbes[2]

[1]King's College London, Institute of Psychiatry, Psychology & Neuroscience, London SE5 8AF, UK

[2]King's College London, Institute of Pharmaceutical Science, London SE1 9NH, UK

[3]Kiel University, Department of Pharmaceutics and Biopharmaceutics, 24118 Kiel, Germany

[4]Intertek-Melbourn, Melbourn SG8 6DN, UK

[5]Nemera, La Verpillière 38292, France

[6]Unilever R&D, Colworth Science Park, Sharnbrook, Bedford, MK44 1LQ, UK

[7]Diabetes Research Group, King's College London, King's College Hospital Campus, Weston Education Central, London, UK

[8]Institute of Diabetes and Obesity, King's Health Partners, London, UK

Journal of Controlled Release

Abstract

This study aimed to characterise three nasal drug delivery devices to evaluate their propensity to deliver human insulin solutions to the nasal cavity for redistribution to the central nervous system. Brain delivery was evaluated using functional magnetic resonance imaging to measure regional cerebral blood flow. Intranasal insulin administration has been hypothesised to exploit nose-to-brain pathways and deliver drug directly to the brain tissue whilst limiting systemic exposure. Three nasal pump-actuator configurations were compared for delivery of 400 IU/mL insulin solution by measuring droplet size distribution, plume geometry, spray pattern and *in vitro* deposition in a nasal cast. The device with optimal spray properties for nose to brain delivery (spray angle between 30° and 45°; droplet size between 20 and 50 µm) also favoured high posterior-superior deposition in the nasal cast and was utilised in a pharmacological magnetic resonance imaging study. Functional magnetic resonance imaging in healthy male volunteers showed statistically significant decreases in regional cerebral blood flow within areas dense in insulin receptors (bilateral amygdala) in response to intranasally administered insulin (160 IU) compared to saline (control). These changes correspond to the expected effects of insulin in the brain and were achieved using a simple nasal spray device and solution formulation. We recommend that a thorough characterisation of nasal delivery devices and qualitative/quantitative assessment of the administered dose is reported in all studies of nose to brain delivery so that responses can be evaluated with respect to posology and comparison between studies is facilitated.
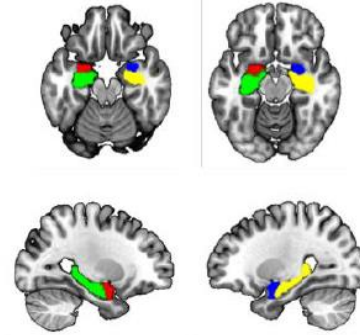
Graphical Abstract
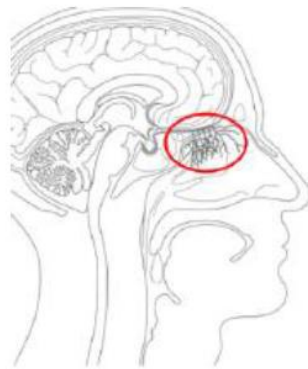
Effects of intranasal Insulin on regional cerebral blood flow
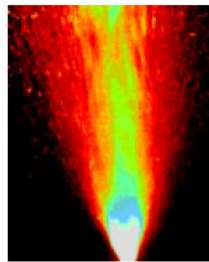
Regions of Interest

● L amygdala   ● R amygdala
● L Hippocampus   ● R Hippocampus

1 Introduction

Given the rising prevalence of diabetes mellitus and metabolic disorders, such as obesity, within the developed world [1] there has been an increase in the number of studies focused on the central nervous system response to insulin [2, 3]. The primary role of insulin in the body is to regulate and maintain normal blood glucose levels through cellular uptake and storage of glucose in skeletal and adipose tissue. In the brain, however, neuronal glucose uptake is insulin independent and insulin is involved with other processes within the brain which are mediated via the insulin receptor, i.e. homeostasis, food appetite regulation, food reward and memory [4, 5]. Nasal administration has been proposed as a means to deliver insulin to the brain to study its effects with limited interference from systemic insulin-glucose interactions. Nose-to-brain delivery bypasses the blood brain barrier (BBB) by transport across olfactory epithelia into the subarachnoid space, effectively reaching brain tissue within 30-60 min [6]. Thus, nasal insulin administration can be utilised as a tool for research in patients with diabetes and obesity where regular receptor-mediated transport of insulin across the BBB to the brain tissue may be disrupted [7, 8].

For optimal nose-to-brain delivery, insulin must be deposited in the upper posterior region of the nasal cavity where the olfactory epithelium is located, Figure 1 [9, 10]. To achieve optimal brain delivery sufficient drug solution must reach the olfactory epithelium deposition site (highlighted in Figure 1), which is situated proximally to the olfactory bulb and cribriform plate. The olfactory receptor neurons, which are thought to provide a pathway for drug transport, are interspersed among supporting cells (sustentacular cells), microvillar cells, and basal cells [10]. Disappointingly, the dose-determining characteristics of delivery systems used to administer insulin in studies to date have not been well characterised or reported. For example, minimal details regarding the nasal device, spray characteristics or deposition pattern are provided in a study demonstrating dose-dependent nose-to-brain insulin absorption [11]. Studies using both *in vitro* nasal casts and computational modelling provide a general framework of nasal pump performance characteristics that are optimal for posterior drug deposition which is necessary for efficient nose-to-brain drug delivery [12-14]. Critical performance parameters have been defined and underpin the guidelines and

regulations for nasal drug products of the regulatory agencies such as the FDA and EMA [15]. Nasal drug deposition is dependent on human factors such as actuation force, actuation angle and nasal anatomy as well as those dictated by the combination of device and formulation such as droplet size, plume angle and plume area. The latter parameters can be measured using *in vitro* methods and serve as proxy measures for predicting spray distribution and deposition in the human nasal cavity. Deposition studies in human cast models provide a simulation of nasal delivery to the human nasal cavity using a realistic anatomy and air flow. For upper nasal cavity drug deposition a device and formulation capable of producing a plume with a small spray angle (between 30° and 45°) and small droplets (between 20 and 50 μm) is desired [12-14].

Locating drug-receptor binding *in vivo* can be conducted using imaging methods such as positron emission tomography, but comes at a large financial cost, requires complex chemistry and is inappropriate for repeated investigations due to radioactive isotope exposure. Magnetic resonance imaging (MRI), on the other hand can be used for repeated measures as illustrated by several recently published pharmacological investigations [16]. An MRI method for pharmacological studies is arterial spin labelling (ASL), which permits measurement of cerebral blood flow (CBF) in quantitative units (ml/100 g/min) in a time of approximately 5-6 min [17]. Following changes in neuronal activity from a stimulus, such as a sensory or cognitive task or pharmacological modulation, the oxygen demand to the stimulated neuronal region is increased. This increase in oxygen is satisfied by an increase in blood flow to that region via vasodilation at the level of the arterioles through a phenomenon known as neurovascular coupling [18]. Therefore, changes in regional CBF (rCBF) which can be measured using ASL reflect changes in physiology that provide a surrogate measure of changes in neuronal activity.

In this study we characterised the spray properties of human insulin solution in two commercially available nasal spray pumps with three types of actuator. The nasal spray performance was evaluated using standard nasal drug product quality attributes [19]. These measurements were droplet size distribution, spray divergence angle/width and spray cross-sectional area/ovality. Furthermore, nasal cavity deposition was compared using an *in vitro* nasal cast for each of the pump configurations look at how well the measured spray properties translated into

5

deposition patterns. The device with the characteristics that most favoured upper and posterior nasal cavity penetration was selected for an evaluation of nose-to-brain delivery in human volunteers by using an MRI method, arterial spin labelling, to measure CBF as a functional biomarker for central insulin delivery. In contrast to most nose-to-brain studies, we provide a detailed characterisation of the nasal delivery device and drug delivered to the nasal cavity.

2 Materials and Methods

Human Insulin (Humulin®, 500 IU/ml) was purchased from Eli Lily, USA. Nasal spray pumps (100 µL) were provided by Nemera (La Verpillière, France), the SP270+® with two crimp-on actuator types (3959 and 4290) and a new prototype device with a single crimp-on nasal actuator (5701) (Figure 2A). The SP270+ pump configurations and new prototype device were filled with 2.5 mL and 4.5 mL of insulin solution (400 IU/mL; Humulin diluted 4:1 with saline 0.9% w/v immediately before administration - viscosity 0.967 ± 0.002 mPa.s at 25°C), respectively.

2.1 Droplet Size Measurement

Droplet size analysis was performed by laser diffraction using a Malvern Spraytec® (Malvern Instruments, Inc, Southborough, MA) and Proveris Vero® (Proveris Scientific Corporation, Malborough, MA) automated actuator for reliable and automated actuation of each pump configuration (n=5/pump). Actuation force was kept constant for all experiments and pump configurations at 6.8 kg. The automated actuator was placed between the laser and the detector lens at 90° to achieve vertical spray actuation. Data was collected at two distances from the tip of the actuator to the middle of the laser beam (30 mm and 60 mm) with single actuation per distance. Data was processed and analysed using the Malvern software. Obscuration values over time were used to identify the stable phase when the plume is most constant, which was selected for analysis. From this phase the particle size cut-offs encompassing 10, 50 and 90% of the total sample volume, the Dv10, Dv50 and Dv90, as well as respirable fraction (% <10 µm) were estimated. Unpaired t-tests were performed between pump configurations to compare droplet size distributions.

2.2 Plume Geometry and Spray Pattern Measurement

A Proveris SprayView® with Proveris Vero® automated actuator (Proveris Scientific Corporation, Malborough, MA) and actuation settings as above were used to assess plume geometry and plume spray pattern. The SprayView setup coupled a high-speed camera and a pulsed laser light sheet to capture high quality images of the insulin plume as it evacuates the pump. The laser light sheet orientation determines what information can be obtained. For plume geometry, the light sheet was positioned to dissect the centre of the plume from a single actuation, parallel to the plume flow. For

spray pattern the light sheet was positioned to dissect the plume at an angle perpendicular to the flow of a single actuation with measurement at distances of 30 and 60 mm.

For each test, using the Proveris software (Viota Software, Proveris Scientific Corporation, Malborough, MA), the image with maximal image intensity, i.e. plume at its largest, was used for analysis. From this image the tip of the nozzle was located and the two arms of the left and right side of the plume were defined using a threshold selection process. The angle between the two arms was measured as well as the distance between the two arms at a point 60 mm away from the tip of the nozzle, these metrics represent plume angle and width, respectively. Using the Proveris software the total spray duration was manually defined using an image intensity graph, and the images selected were then used to analyse and calculate the area (mm^2), defined as the area bounded by the spray pattern contours, as well as ovality. Ovality is a ratio of the D*max* (the longest distance across the plume) and D*min* (the longest width across the plume). Absolute ovality would give a value of 1, where *Dmax=Dmin*.

2.3 Nasal Cast Deposition

The nasal cast model (Boehringer Ingelheim Pharma GmbH & Co. KG, Ingelheim, Germany) used for these experiments was made from CT scan data of a complete adult human nose [20]. The cast consists of five parts representing nostrils, nasal vestibule, lower turbinates, middle and upper turbinates and nasopharynx (Fig 4a). At the end of the nasal cast a filter was used to collect the post-nasal fraction possibly reaching the lung. The nasal cast was operated with inspiration flow of 15 L/min generated by a vacuum pump connected to the filter holder at the rear end of the cast. The insulin solution (400 IU/mL) was administered to the cast using three nasal pump-actuator configurations. Approximately 2.5 mL or 4 mL of insulin solution were filled into reservoir of the device and with each shot a single dose of 100 µL was delivered from the device. The nasal spray was inserted into the nostrils of the cast at an angle and penetration depth to mimic the administration procedure in the human volunteer study. Two sprays into each nostril for each determination were delivered at an angle of 45° parallel to the septum. As liquid sprays are not susceptible to particle bounce the cast was not coated, but was dissembled immediately after administration of the sprays to minimise any opportunity for redistribution of the deposited dose. Use of a

8

concentrated insulin solution permitted administration of 400 µL spray which is less likely to result in run-off than higher volumes that are sometimes used, e.g. 1.6 mL [11]. Regional deposition was reproducible and no visible liquid pooling or signs of redistribution were observed. Individual cast segments were rinsed with 10 mL water to recover the insulin deposited in the nasal cast, which was measured by HPLC assay with all determinations performed in triplicate.

A Waters 2796 Separations Module HPLC was used, equipped with Waters 2489 Photodiode Array Detector. The column was Thermo Scientific Hypersil 3 µm Hypurity Advance 150 × 4.6 mm RP8. Data were digitalized by Empower program (Waters, Elstree, UK) for chromatograms and integration. The column temperature was set at 25°C and the UV detection wavelength used at 214 nm. An isocratic mobile phase consisting of phosphate buffered saline (PBS) and acetonitrile (70:30 *v/v*), degassed was used in the HPLC analysis. The flow rate of 1 mL/min and pressure limit of 1100 were set with injection volume of 100 µL. Samples were analysed in duplicate with run time of 8 min. The calibration curve was constructed by the standard insulin solution and it was used to quantify each sample peak obtained. Stock solution of insulin (5 mg/mL) was prepared and serial dilutions (0.65, 1.25, 2.5, 5, 10, 20, 40, 80 µg/mL) were performed for construction of calibration curve.

2.4 Human Volunteer Study

2.4.1 Participants

The device determined by *in vitro* studies to be most suitable for nose to brain delivery was selected for use in a double-blind randomised crossover fMRI study to investigate the effect of insulin on cerebral blood flow. Here we report the data that provide evidence for delivery of insulin to the brain (changes in cerebral blood flow after administration of insulin compared to saline placebo) and systemic circulation (biochemical measures) following intranasal administration. Sixteen healthy male volunteers were recruited (age= 24.67 ± 4.30, mean ± SD). All participants visited three times in total, once for a screening session followed by two scanning visits separated by at least seven days. All eligible participants had a body mass index (BMI) between 25-31.4 kg/m^2 (BMI=27.76 ± 1.92), had no history of psychiatric illness or diabetes assessed by clinical interview, no cardiac complications as assessed by

electrocardiogram (ECG), no history of any eating disorders, asthma or allergies associated with breathing difficulties and did not adhere to a vegetarian or vegan diet. All subjects were also screened for any MR contraindications. This study was approved the King's College London Psychiatry Nursing and Midwifery Ethics Committee (ethics no. RESCM-17/18-2282).

On both scanning visits participants arrived following an overnight fast (approx. 12 hours). Blood samples were collected before and after scanning (pre dose and post scan) and were assessed for plasma glucose, serum insulin and serum C-peptide concentrations.

2.4.2 Drug Administration

Twenty minutes prior to being loaded into the scanner participants received either 160 IU insulin (400 IU/mL) or saline solution 0.9% w/v (control)) via intranasal application using the SP270+ pump and 3959 actuator. Administration was approximately thirty minutes prior to functional data acquisition in an effort to acquire data after insulin concentrations in the central nervous system had increased in accordance with the pharmacokinetics of intranasal insulin previously reported [21].

Participants were familiarised with intranasal application and self-administered the dose under instruction from the lead investigator. The nozzle was inserted into a nostril parallel to the septum at the same penetration depth and angle utilised for the nasal cast. Participants received a total of 4 spray doses (i.e., 4 x 100 µL x 400 IU/mL), alternating between nostrils and leaving one minute between each spray nostrils. Participants took a forward leaning position and used their left hand to administer to the right nostril and vice versa. Following each spray, participants were instructed to hang their head down and forward to prevent any drug loss to the nasopharynx nasal and take advantage of gravitational forces to direct any transport towards the upper turbinates and olfactory regions of the nasal cavity.

2.4.3 MRI acquisition, Image Processing and Analysis

All scanning was conducted using a MR750 3 Tesla GE Scanner with a 32 channel head coil. High resolution anatomical images were acquired to permit spatial standardisation of functional data. Resting cerebral perfusion images (functional data)

were collected using a 3D pseudo-continuous arterial spin labelling (pCASL) sequence acquired at a resolution of 2.96 x 2.96 x 3 mm^3 in a time of 5:22 min. During perfusion image acquisition participants were asked to keep their eyes open and look at a cross displayed to them on the screen.

Quantitative maps of CBF were computed from perfusion weighted images using the scanner software, implementing the model recommended by the ASL White paper [22]. Anatomical images were used to create a group template using Advanced Normalistion Tools (ANTs, templatecreate.sh, [23]) which was registered to standardised space through FSL's FLIRT [24, 25] (FSL, FMRIB, version 3.20, University of Oxford, UK, http://www.fmrib.ox.ac.uk/fsl). All individual subject transformations and warp parameters from these steps were saved. CBF maps were co-registered to the anatomical images using epi_reg (FSL). Individual CBF maps were registered to standardised space by applying the saved transformations and warps using ANTs.

To assess insulin induced changes in global perfusion whole brain median grey matter (GM) CBF values, constrained to a standardised GM mask, were extracted from the processed CBF maps and compared using a paired t-test, judged to $p < 0.05$ significance. In order to ascertain group level changes in CBF we extracted median values from regions of interest (ROI) for each participant and condition. Regions known to possess insulin receptors were created into masks using the FWU pick atlas toolbox, with the AAL human atlas in SPM (SPM-12, Wellcome Trust Centre for Neuroimaging, University College London, UK, http://www.fil.ion.ucl.ac.uk/spm). These regions where the left and right hippocampus and amygdala, respectively, (see figure 3) which were picked due to the presence of insulin receptors within these regions [26].

2.4.4 Blood insulin, C-peptide and glucose concentration

Venous blood was collected prior to administration of either insulin or saline (pre-dose) and immediately after the scanning protocol was completed (post-scan). The duration between these two time points was approximately two hours. Blood was collected by venepuncture from the cubital vein. Blood was collected into plasma and serum separating vacutainers (two vacutainers in total). These samples were centrifuged,

and plasma and serum was extracted into aliquots for analysis.   Biochemical analysis was performed for serum insulin and C-peptide (Siemens Healthcare Centaur Assays) and plasma glucose (Siemens Healthcare AVIDA).

2.5 Data analysis

Data for the nasal spray characterisation is presented as mean ± sd,   Statistical analysis was conducted using R statistical analysis software (Rstudio – version 1.1453, Boston, MA, http://www.rstudio.org/). As mentioned in the relevant sections above unpaired t-tests were performed between pump configurations to compare droplet size distributions, plume geometry and spray pattern analysis. For the spray pattern analysis a Mann Whitney Test for unpaired samples was used for spray pattern measures at 60 mm P values were judged to $p < 0.05$ and $p < 0.01$ significance. For nasal cast deposition analysis a two way analysis of variance (ANOVA) model was constructed with a Bonferroni post hoc test and p values < 0.05 were considered statistically significant.

Plasma glucose, serum insulin and serum C-peptide measurements, pre dose and post scan, were tested for statistical differences using paired t-tests for each condition. P values were judged to $p < 0.05$ significance. For the MRI data, the extracted CBF values were statistically compared to look for treatment related differences (insulin vs saline placebo) in regional CBF using a paired t-test for each ROI, a p value of 0.05 was used as a threshold of significance for this analysis.

3. Results

The three devices for nasal delivery of insulin solution were evaluated in terms of the emitted aerosol spray characteristics (dosimetry, droplet size, spray geometry, *in vitro* deposition), after which the device with the optimal deposition pattern was evaluated for induction of changes in regional cerebral blood flow in humans in response to intranasal administration of insulin.

3.1 Spray droplet size

The pump configurations and are illustrated in Figure 2. Spray droplet size was evaluated for each pump data (Figure 2; table 1). No significant differences in Dv10, 50 or 90 were seen between 3959 or 4290 at 30 mm. Significant differences were seen between 3959 and Prototype at 30 mm: mean difference = -5.9 μm, -22.9 μm and -50.8 μm, for Dv10 ($p<0.05$), Dv50 ($p<0.05$) and Dv90 ($p<0.001$), respectively. Significant differences were also seen between 4290 and Prototype at 30 mm: mean difference =-7.8 μm, -26.2 μm and -55.6 μm, for Dv10 ($p<0.001$), Dv50 ($p<0.001$) and Dv90 ($p<0.001$), respectively. Furthermore, droplet size distribution at 60 mm differed between all the devices with the 4290 producing the smallest and the Prototype producing the largest droplets. Potential respirable fractions (droplets < 10 μm) for all pump configurations were very low; < 1.5% for all devices.

3.2 Plume Geometry and Spray Pattern

Representative images of the spray profile for each device are displayed in Figure 4, along with average plume angle and width parameters. No significant differences were seen between the 3959 and 4290 devices for either plume angle or width. Significant differences were seen for plume angle and width between the 3959 device (mean ± sd = 37.8 ± 3.9° and 41.3 ± 4.6 mm, respectively) and the Prototype device (mean ± sd = 27.5 ± 7.8° and 29.9 ± 8.9 mm, respectively). Similarly, significant differences between the 4290 device (mean ± sd = 42.7 ± 3.7° and 47.3 ± 4.6 mm, respectively) and the Prototype device were observed.

Spray pattern images were analysed and measurements of the spray area and spray ovality are presented in Figure 4C and D. Spray pattern measurements for the devices at 30 mm and 60 mm were compared using the Mann Whitney test for unpaired data

13

(n=4). There was no significant difference between the spray area produced by the devices at either height. The 4290 configuration produced higher ovality scores (more elliptical) compared to both the 3959 and the Prototype at 60 mm, but the differences were small.

3.3 In vitro deposition

A nasal cast (Figure 5a) was used to evaluate the deposition of insulin from the three nasal pump-actuator configurations. Insulin solution was recovered from almost all of the nasal cast sections (Figure 5b), with slightly different deposition profiles for each of the three nasal pump-actuator combinations. The highest deposition was in the nasal vestibules for all configurations with significant difference in the proportion of dose deposited between 3959 and the Prototype (mean ± sd = 47.1 ± 2.8% vs 78.9 ± 3.7%, $p < 0.001$). Insulin deposition in the middle / upper turbinates section of the cast, i.e. the section where the target olfactory epithelium is located, was 17.9 ± 7.1%, 16.7 ± 6.1% and 4.7 ± 4.2% for the 3959, 4290 and Prototype, respectively. Less than 0.1% of the formulation from all nasal pump-actuator configurations passed through the nasal cast model to constitute an inhalable fraction to the lungs.

3.4 Magnetic Resonance Imaging

The 3959 actuator with SP270+ pump was used for the magnetic resonance imaging component of this work. All subjects were compliant with the drug administration protocol and handled the 3959 configured nasal spray device competently. No adverse effects were reported for either intranasal saline or insulin formulations. One subject was excluded from the analysis for failure to comply with the fasting protocol (detected on the basis of pre-dose administration 'fasting' blood insulin concentration greater than 50 mIU/L) and therefore the MRI analysis and hunger rating analysis was conducted on the fifteen remaining participants. Due to issues with blood sampling for a further individual subject, blood analysis was only conducted on fourteen subjects.

There were no significant changes in plasma glucose, serum insulin or serum C-peptide at either pre-dose or post scan time points after insulin treatment compared to saline control (table 2). In some participants treated with insulin a small decrease in blood glucose was detected in combination with a small rise in insulin, however this

14

effect was not statistically significant between insulin and saline administration when analysed for whole study. For both insulin and control arms of the study there was a significant effect of time on serum C-peptide concentration which significantly decreased between the pre-dose and post scan measurement times ($p = 0.015$ and $p = 0.013$, for saline placebo and insulin, respectively).

3.5 Central Effects of Intranasal Insulin

Paired t-tests from CBF values extracted from the global grey matter revealed no difference between conditions (table 3). For regional CBF assessment both the left and right amygdala structures revealed significant CBF decreases in response to intranasal insulin ($p= 0.037$ and 0.027, respectively). Slight CBF decreases in response to insulin were detected from the left and right hippocampal ROIs but were not statistically significant (mean decrease = 2.14 ml/100 g/min and 2.38 ml/100 g/min, $p = 0.32$ and $p = 0.24$, for saline placebo and insulin, respectively).

4. Discussion

This was a comparative study that analysed the insulin solution spray characteristics of three commercial, nasal pump delivery device configurations. This study has determined pump performance in terms of the nasal deposition and used *f*MRI to study the CNS effects of intranasal insulin in human volunteers. *A priori* criteria to select the best pump were droplet size between 20 μm and 50 μm contained in a narrow plume between 30° and 45° [12-14].

The nasal cast data showed obvious deposition differences between the different pump configurations. All pumps delivered high deposition in the nasal vestibule and at the expense of deep penetration into the nasal cavity. This is a typical deposition profile of a normal liquid nasal spray [27]. However, the 3959 and SP270+ configuration showed the least nasal vestibule deposition and the highest deposition within the lower, middle and upper turbinates in comparison to the two other tested pumps with a more evenly distributed deposition across the nasal cast regions. As inferred from the droplet size data, the prototype device, which had considerably larger droplets, deposited mainly at in the nasal vestibule. The high inertia carried by these larger droplets favours increased impaction in anterior regions and reduced ability for the plume to navigate the convoluted anatomy of the nasal cast and cavity. The 4290 with SP270+ configuration showed similar characteristics to the 3959 but differed significantly with regards to nasal cast deposition at the level of the nasal vestibule and lower turbinate. This deposition profile may be related to the plume angle associated with this pump resulting in more deposition in anterior regions of the nasal cast model.

These data indicate that the SP270+ with both 3959 and 4290 actuators produced well developed plumes with characteristics that met the *a priori* criteria. A narrow plume with larger droplets, such as that demonstrated by the Prototype, acts like a jet/hose rather than a mist which is sub-optimal for upper nasal cavity deposition, making it less efficient for nose-to-brain delivery of insulin. The SP270+ with 3959 and 4290 actuators produced sprays with favourable characteristics for the intended use. Droplet size distributions at 30 mm were equivalent for both pumps with over 50% in the target 20-50 μm range. The measured plume angle and ovality at 30 mm was

16

similar for both devices, producing sprays in the range of 30-45°. As the plumes were no different at 30 mm, a distance more anatomically relevant than 60 mm, device manoeuvrability and ease of use were used as supplementary criteria to select a device for use in the human study. The 3959 actuator was considered to have ergonomic advantages, due to the finger grips and shape providing an easier handling during actuation which may result in more reproducible use by human volunteers in the imaging study. Thus, the SP270+ pump with the 3959 actuator was selected for use in the MRI study of the central effects of nose-brain insulin in humans. It is intriguing to speculate whether the differences in the performance of the nasal delivery devices types would have manifested in measurable differences in response to delivery of insulin to the brain, but this was unfortunately beyond the scope of this investigation.

All subjects used the nasal spray device competently and had no problems following the administration protocol. When insulin was administered, there were small increases in serum insulin concentration in some participants which has been reported previously with this dose and is an effect of overspill into the peripheral circulation [11]. However, serum insulin concentrations were not significantly different when participants were administered insulin compared to saline when the study was analysed collectively. There was a small reduction in plasma glucose concentration associated with the participants for whom insulin levels were raised, although this too was not statistically significant as an effect of treatment. The decrease in C-peptide over the duration of the study was observed for insulin- and saline-treated participants and represents a normal decrease in c-peptide release during periods of fasting. As serum insulin, glucose and c-peptide varied minimally in response to treatment, and differences were statistically insignificantly overall, it was considered that the changes in CBF were responses to insulin transported to the CNS via nose to brain delivery rather than the result of secondary insulin transportation to the CNS after systemic absorption.

The functional relationship between neural activity and CBF permitted the use of ASL MRI to explore brain function using CBF as a surrogate measure and was used to assess the central effects of intranasal insulin [28]. ASL works by magnetically tagging or labelling the hydrogen nuclei of water molecules within the major feeding arteries

of the brain (carotid arteries), waiting for these tagged molecules to reach the capillary bed of the brain tissue and then acquiring an image. This is called a tagged image. A second image is acquired with identical parameters, but in this case with no labelling of arterial blood, known as a control image. The two images are subtracted from each other to remove the static tissue signal and what remains is an image with signal related entirely to the volume of labelled water molecules that have perfused into the tissue to produce a perfusion weighted image [29, 30]. From these perfusion weighted images, a map of CBF in physiological units can be calculated using a suitable model [31]. These maps were used to study differences in regional CBF within this study.

We report no change in global CBF in response to insulin, an observation witnessed previously [32]. Despite the exclusion of one of the participants from the analysis we had sufficient statistical power to detect a significant treatment group level decrease in CBF in response to 160 IU insulin compared to saline placebo in the left and right amygdala. From pre-clinical and *in vitro* literature the central nucleus of the amygdala expresses an abundance of insulin receptors [33]. Binding of insulin to these receptors has been shown to selectively increase both the amplitude and frequency of spontaneous inhibitory postsynaptic currents [33]. The consequent reduction in oxygen demand in the amygdala leads to lower cerebral perfusion. Previous reports have shown decreases in CBF associated with 160 IU intranasal insulin dose in the hypothalamus [11], but no study has reported changes within the amygdala, a region that is involved in food intake and appetite control [34]. Interestingly, direct administration of insulin to the amygdala in rats has previously shown an acute reduction in food intake coupled with reduced appetite [35]. Previous reports have identified an hunger or appetite blunting effect following intranasal insulin administration [36, 37] and the results reported here may offer a possible explanation for these anorectic effects.

5. Conclusion

As a proof of concept we have, through the use of functional MRI, shown that a commercial nasal pump can be used to deliver insulin within the nasal cavity to produce a pharmacological effect in the brain of healthy human volunteers. This is the first time that a nasal pump with human insulin has been characterised fully in terms of aerosol delivery and used in a human magnetic resonance imaging study. Thus, our results provide evidence of successful nose-to-brain delivery of insulin to engage brain insulin receptors resulting in changes in cerebral perfusion within the amygdala.

We have shown that a commercial nasal pump with human insulin can be used to induce measurable effects within the central nervous system. This constitutes a simple, cost effective means of administration for centrally acting drugs for use in neuropharmacological research, biomedical applications or therapeutic interventions. The delivery device used for this purpose was not optimised and the insulin solution was not modified to target olfactory delivery. We recommend thorough characterisation of the nasal delivery device and qualitative/quantitative assessment of the administered dose is reported in all studies of nose to brain delivery so that responses can be evaluated with respect to posology and comparison between studies is facilitated.

19

Table 1 Droplet size measurements obtained from each pump measured at 30 mm and 60 mm from the tip of the actuator. Data is mean ± sd (n=5)

| | | Droplet Size in µm: 30 mm Distance | | |
		3959	4290	Prototype
30 mm	Dv10	18.03 ± 2.95	23.98 ± 3.86	23.98 ± 3.86
	Dv50	37.20 ± 2.20	60.06 ± 16.27	60.06 ± 16.27
	Dv90	76.34 ± 3.79	71.52 ± 13.34	127.14 ± 29.77
		Droplet Size in µm: 60 mm Distance		
		3959	4290	Prototype
60 mm	Dv10	21.80 ± 1.58	19.40 ± 4.08	28.72 ± 2.87
	Dv50	39.65 ± 0.10	34.95 ± 1.33	56.50 ± 11.32
	Dv90	69.56 ± 1.69	61.02 ± 3.35	111.67 ± 31.28

The measured droplet size differed between pumps and these statistical comparisons are represented in Figure 2.

Table 2 Measurements of plasma glucose, serum insulin, C-peptide, pre-dose and post-scan, following intranasal administration of insulin 160 IU/mL and saline 0.9% w/v (control). Data represent mean ± sd, n=14 (one participant did not have complete blood data), and show significant p values (*) calculated from paired t-tests (p < 0.05).

	Peripheral Blood Analysis			
	Saline		Insulin	
	Pre	Post	Pre	Post
Plasma Glucose (mmol/L)	4.99 ± 0.32	4.95 ± 0.31	4.99 ± 0.38	4.82 ± 0.41
Serum Insulin (mIU/L)	6.99 ± 3.85	6.64 ± 4.71	9.76 ± 8.27	16.79 ± 13.48
Serum C-peptide (pmol/L)	496.57 ± 166.25	* 434.50 ± 155.40	487.29 ± 170.35	* 338.57 ± 144.98

- Denotes significant differences between pre-dose and post-scan measurements (p< 0.05)

Table 3. Global and regional cerebral blood flow values extracted from the grey matter and amygdala and hippocampus, respectively for both saline and insulin conditions. CBF values are reported as mean ± sd and were compared across conditions using paired t-tests and significance was defined as p < 0.05 *, n=15.

| Global and regional Cerebral Blood Flow (ml/100 g/min)		
	Saline	Insulin
Grey matter	59.19 ± 5.83	**59.60 ± 4.98**
Amygdala		
Left	46.68 ± 5.72	42.72 ± 6.97
Right	44.85 ± 6.07	40.80 ± 6.57
Hippocampus		
Left	45.98 ± 4.49	43.84 ± 5.75
Right	45.66 ± 4.17	43.27 ± 5.83
* Denotes significant insulin related decreases compared to saline (p< 0.05)		
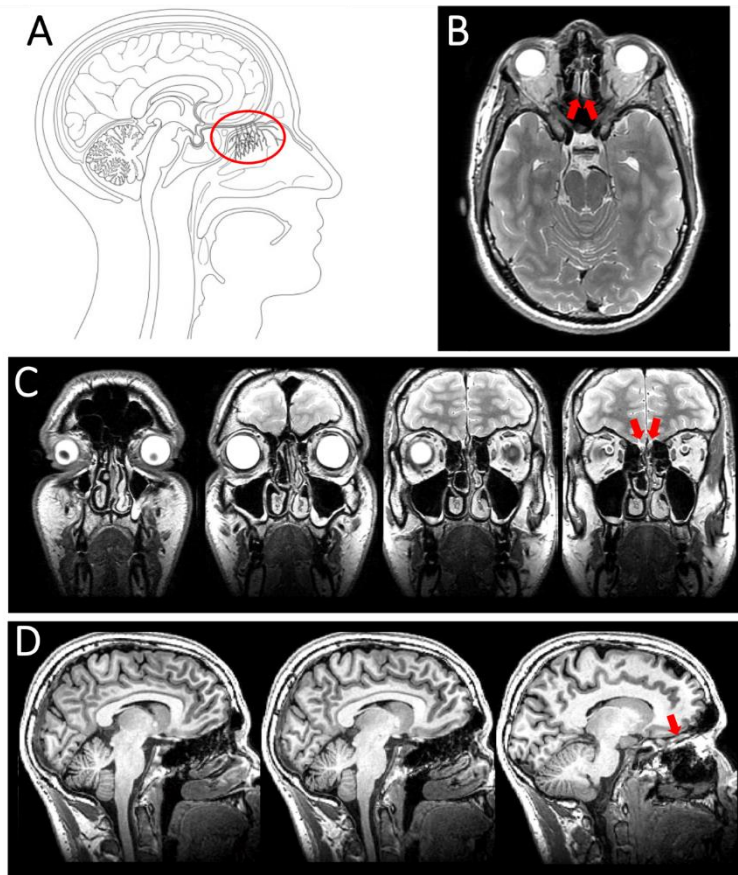
Figure 1. Schematic drawings and anatomical MRI images of the olfactory bulb and nerve fibres within the nasal cavity and central nervous system. A) schematic diagram of the olfactory bulb and olfactory nerve fibres that breach the cribriform plate (circled in red). B) An axial T2 weighted image from a representative subject showing the olfactory bulb (red arrows). C) Coronal T2 weighted images show the intricacy of the nasal cavity and also the olfactory bulbs (red arrows). D) Sagittal T1 weighted image of the same representative subject showing the olfactory bulb lying superior to the cribriform plate (red arrow).
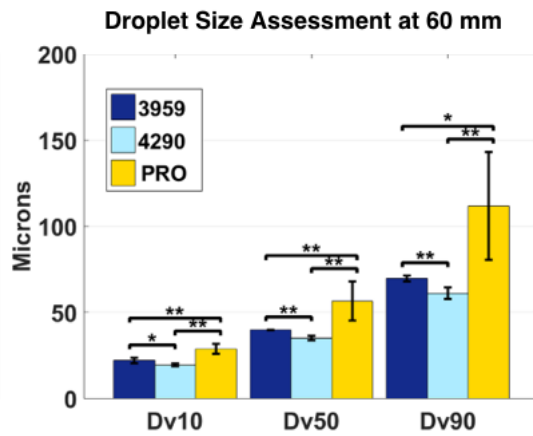
A

B
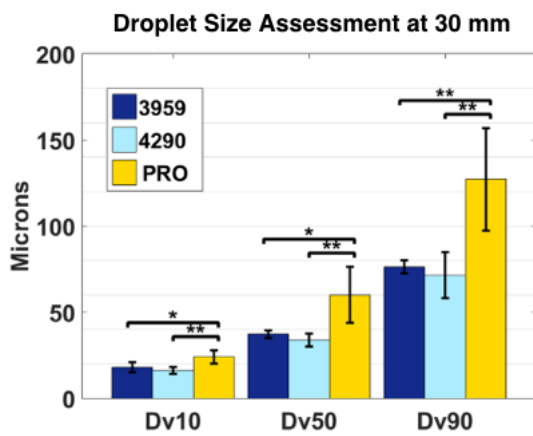
C

Figure 2. Nasal spray devices and aerosol particle size distributions. (A) The SP270+ pump with 3959 or 4290 actuator and a prototype (PRO) pump; (B) droplet size at 30 mm, (C) droplet size at 60 mm. Data represent mean ± sd (n=5).
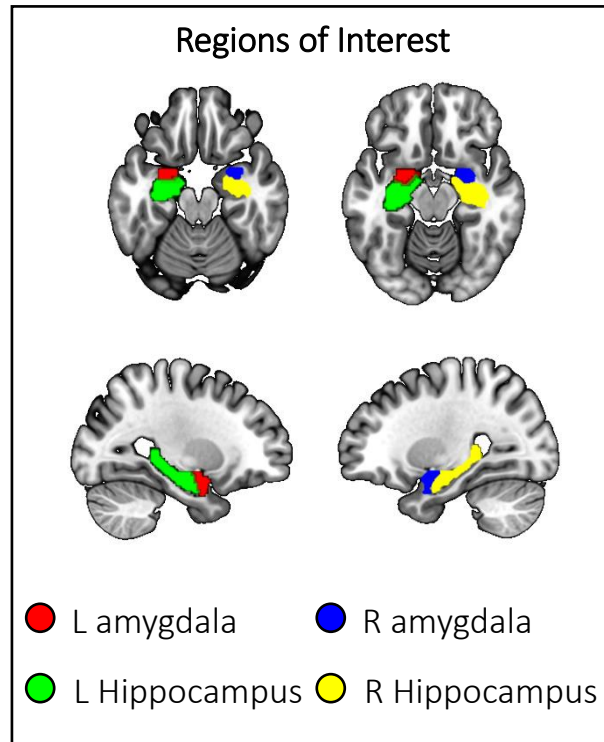
Figure 3. Amygdala and hippocampal region of interest masks. The amygdala and hippocampus were used as regions of interest to explore effects of intranasal insulin on perfusion, overlaid onto a standard anatomical brain in MNI space.
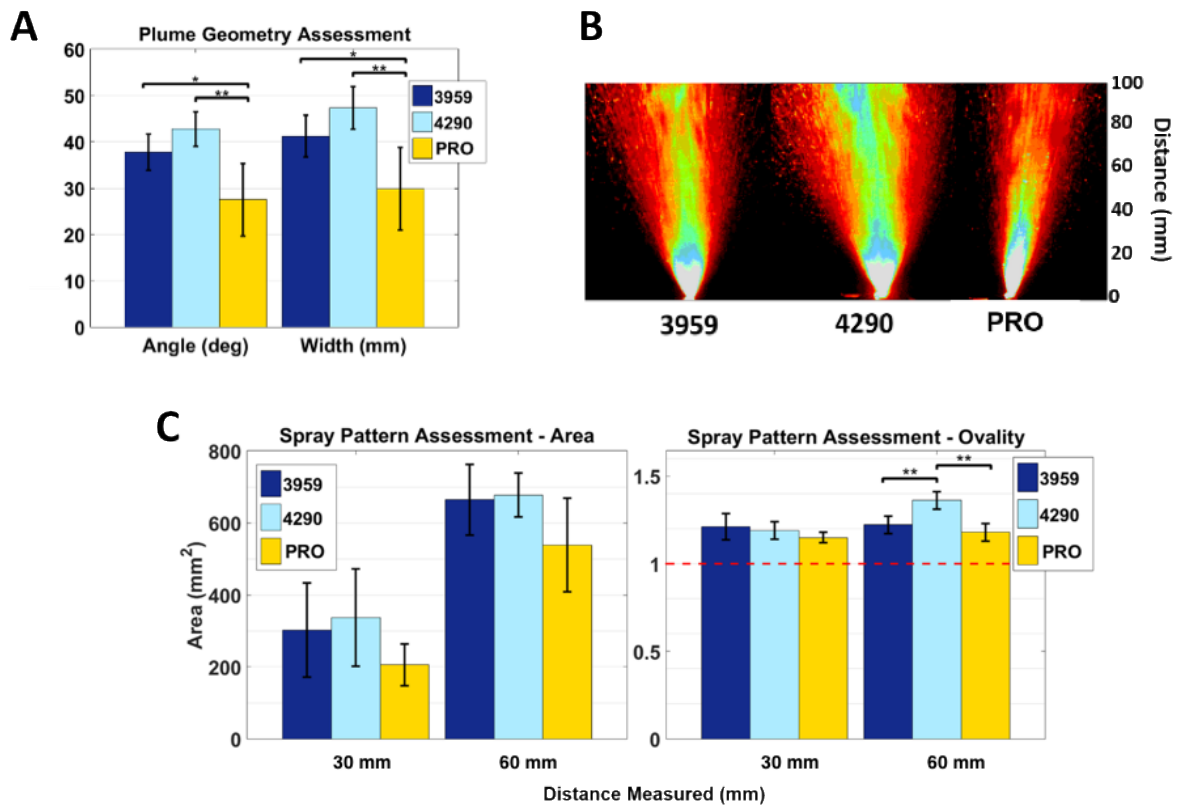
Figure 4. Aerosol geometry of SP270+ pump with 3959 or 4290 actuator and a prototype (PRO) pump. (A) plume angle and width at 60 mm, (B) representative images of a stable phase plume. Data represent mean ± sd (n=5); (C) plume area (mm^2) and (D) ovality measurements at 30 and 60 mm. The red dashed line represents the line of absolute ovality =1. Data represent mean ± sd (n=5 for 3959,4290 and n=4 for prototype). *p<0.05 and **p<0.01.
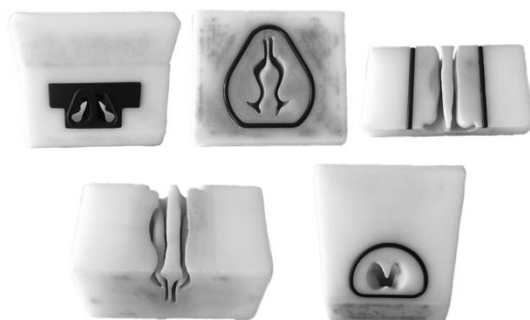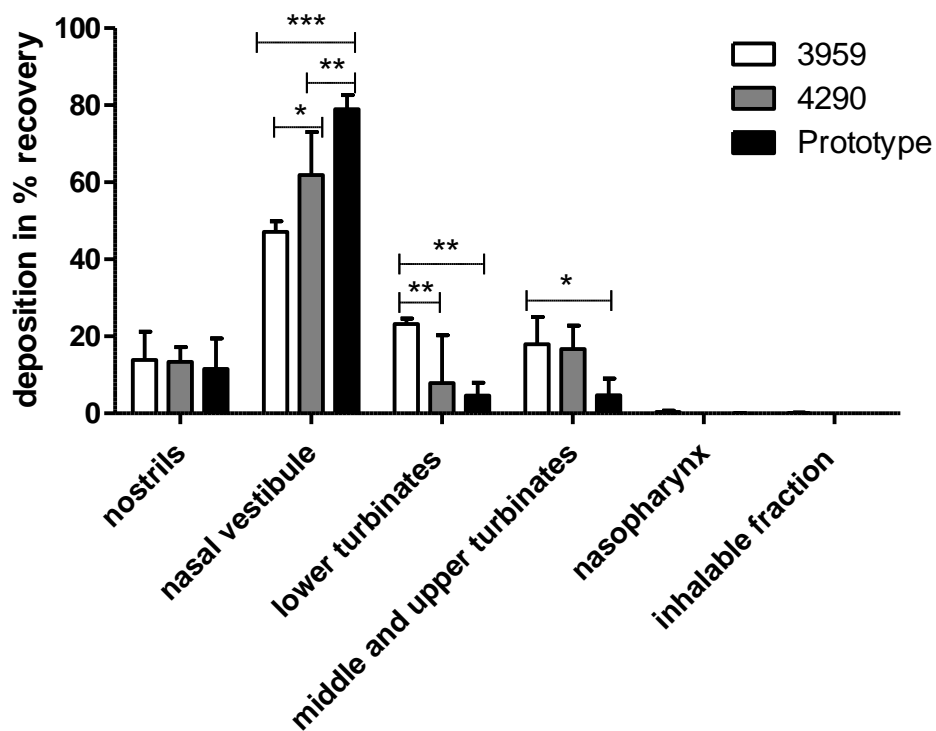
A

B

Figure 5. *In vitro* deposition in the upper turbinate for nose to brain transport: (a) The nasal cast sections (from top left: nostrils, nasal vestibule, lower turbinates; from bottom left: middle and upper turbinates, nasopharynx), (b) deposition fractions in the target area of nostrils, nasal vestibules, lower turbinates, middle and upper turbinates, nasopharynx for insulin aerosols from SP270+ pump with 3959 or 4290 actuator and a prototype (PRO) pump, respectively. Data represent mean ± sd (n=9). *p<0.05, **p<0.01, ***p<0.001

References

1. Bhupathiraju, S.N. and F.B. Hu, *Epidemiology of Obesity and Diabetes and Their Cardiovascular Complications.* Circulation Research, 2016. **118**(11): p. 1723-1735.
2. Heni, M., et al., *Impaired insulin action in the human brain: causes and metabolic consequences.* Nat Rev Endocrinol, 2015. **11**(12): p. 701-11.
3. Heni, M., et al., *Evidence for altered transport of insulin across the blood-brain barrier in insulin-resistant humans.* Acta Diabetol, 2014. **51**(4): p. 679-81.
4. Kido, Y., J. Nakae, and D. Accili, *Clinical review 125: The insulin receptor and its cellular targets.* J Clin Endocrinol Metab, 2001. **86**(3): p. 972-9.
5. Wilcox, G., *Insulin and Insulin Resistance.* Clin Biochem Rev, 2005. **26**(2): p. 19-39.
6. Banks, W.A., J.B. Owen, and M.A. Erickson, *Insulin in the brain: There and back again.* Pharmacology & Therapeutics, 2012. **136**(1): p. 82-93.
7. Craft, S., et al., *Cerebrospinal fluid and plasma insulin levels in Alzheimer's disease: relationship to severity of dementia and apolipoprotein E genotype.* Neurology, 1998. **50**(1): p. 164-8.
8. Kullmann, S., et al., *Selective Insulin Resistance in Homeostatic and Cognitive Control Brain Areas in Overweight and Obese Adults.* Diabetes Care, 2015. **38**(6): p. 1044-1050.
9. Khan, A.R., et al., *Progress in brain targeting drug delivery system by nasal route.* Journal of Controlled Release, 2017. **268**: p. 364-389.
10. Dhuria, S.V., L.R. Hanson, and W.H. Frey, 2nd, *Intranasal delivery to the central nervous system: mechanisms and experimental considerations.* J Pharm Sci, 2010. **99**(4): p. 1654-73.
11. Kullmann, S., et al., *Dose-Dependent Effects of Intranasal Insulin on Resting-State Brain Activity.* J Clin Endocrinol Metab, 2018. **103**(1): p. 253-262.
12. Cheng, Y.S., et al., *Characterization of nasal spray pumps and deposition pattern in a replica of the human nasal airway.* J Aerosol Med, 2001. **14**(2): p. 267-80.
13. Inthavong, K., et al., *A Numerical Study of Spray Particle Deposition in a Human Nasal Cavity.* Aerosol Science and Technology, 2006. **40**(11): p. 1034-1045.
14. Newman, S.P., F. Moren, and S.W. Clarke, *Deposition pattern of nasal sprays in man.* Rhinology, 1988. **26**(2): p. 111-20.
15. Trows, S., et al., *Analytical challenges and regulatory requirements for nasal drug products in europe and the u.s.* Pharmaceutics, 2014. **6**(2): p. 195-219.
16. Zelaya, F.O., et al., *MR and CT Perfusion and Pharmacokinetic Imaging: Clinical Applications and Theoretical Principles, Chapter 72: Perfusion in Pharmacologic Imaging.* 2016: Lippincott Williams and Wilkins; 1 Har/Psc edition
17. Jenkins, B.G., *Pharmacologic magnetic resonance imaging (phMRI): Imaging drug action in the brain.* NeuroImage, 2012. **62**(2): p. 1072-1085.
18. Attwell, D. and C. Iadecola, *The neural basis of functional brain imaging signals.* Trends Neurosci, 2002. **25**(12): p. 621-5.
19. FDA, U.S.F.a.D.A., *Guidance for industry: Bioavailability and Bioequivalence Studies for Nasal Aerosols and Nasal Sprays for Local Action.* 2003.
20. Schönbrodt, T., et al., *Method development for deposition studies in a nasal cast*, in *Respiratory Drug Delivery 2010*, R.N. Dalby, Editor. 2010, Davies Healthcare International Publishing: Orlando, Florida. p. 445-449.
21. Born, J., et al., *Sniffing neuropeptides: a transnasal approach to the human brain.* Nat Neurosci, 2002. **5**(6): p. 514-6.
22. Alsop, D.C., et al., *Recommended Implementation of Arterial Spin Labeled Perfusion MRI for Clinical Applications: A consensus of the ISMRM Perfusion Study Group and the European Consortium for ASL in Dementia.* Magnetic resonance in medicine, 2015. **73**(1): p. 102-116.
23. Avants, B.B., et al., *A reproducible evaluation of ANTs similarity metric performance in brain image registration.* NeuroImage, 2011. **54**(3): p. 2033-2044.
24. Jenkinson, M., et al., *Improved optimization for the robust and accurate linear registration and motion correction of brain images.* Neuroimage, 2002. **17**(2): p. 825-41.
25. Jenkinson, M. and S. Smith, *A global optimisation method for robust affine registration of brain images.* Med Image Anal, 2001. **5**(2): p. 143-56.
26. Bruning, J.C., et al., *Role of brain insulin receptor in control of body weight and reproduction.* Science, 2000. **289**(5487): p. 2122-5.
27. Kundoor, V. and R.N. Dalby, *Assessment of Nasal Spray Deposition Pattern in a Silicone Human Nose Model Using a Color-Based Method.* Pharmaceutical Research, 2010. **27**: p. 30-36.
28. Hawkins, P.C.T., et al., *An investigation of regional cerebral blood flow and tissue structure changes after acute administration of antipsychotics in healthy male volunteers.* Hum Brain Mapp, 2018. **39**(1): p. 319-331.

29.   Alsop, D.C., et al., *Recommended implementation of arterial spin-labeled perfusion MRI for clinical applications: A consensus of the ISMRM perfusion study group and the European consortium for ASL in dementia.* Magn Reson Med, 2014.

30.   Alsop, D.C. and J.A. Detre, *Multisection cerebral blood flow MR imaging with continuous arterial spin labeling.* Radiology, 1998. **208**(2): p. 410-6.

31.   Buxton, R.B., *Quantifying CBF with arterial spin labeling.* J Magn Reson Imaging, 2005. **22**(6): p. 723-6.

32.   Grichisch, Y., et al., *Differential effects of intranasal insulin and caffeine on cerebral blood flow.* Hum Brain Mapp, 2012. **33**(2): p. 280-7.

33.   Korol, S.V., et al., *Insulin enhances GABAA receptor-mediated inhibitory currents in rat central amygdala neurons.* Neurosci Lett, 2018. **671**: p. 76-81.

34.   Figlewicz, D.P., A. MacDonald Naleid, and A.J. Sipols, *Modulation of food reward by adiposity signals.* Physiol Behav, 2007. **91**(5): p. 473-8.

35.   Boghossian, S., et al., *High-fat diets induce a rapid loss of the insulin anorectic response in the amygdala.* American Journal of Physiology-Regulatory, Integrative and Comparative Physiology, 2009. **297**(5): p. R1302-R1311.

36.   Hallschmid, M., et al., *Postprandial Administration of Intranasal Insulin Intensifies Satiety and Reduces Intake of Palatable Snacks in Women.* Diabetes, 2012. **61**(4): p. 782-789.

37.   Jauch-Chara, K., et al., *Intranasal insulin suppresses food intake via enhancement of brain energy levels in humans.* Diabetes, 2012. **61**(9): p. 2261-8.